SUMMARY OF THE RESULTS FROM THE PHEBUS FPT-1 TEST FOR A SEVERE ACCIDENT AND THE LESSONS LEARNED WITH MELCOR

JONG-HWA PARK*, DONG-HA KIM and HEE-DONG KIM
Korea Atomic Energy Research Institute,
150 Deokjin-dong, Yuseong-gu, Daejeon, 305-353, Korea
*Corresponding author. E-mail : jhpark3@kaeri.re.kr

Received August 18, 2005
Accepted for Publication July 12, 2006

The objectives of this paper are twofold to summarize the new findings and confirmed results from the Phebus FPT-1 experimental data and to report useful information to MELCOR users regarding the better use of MELCOR.

For the core damage behavior, the early stage of a melt progression was predicted well; however, the late phase models, concerned with fuel dissolution, oxide cladding failure, fuel slumping, rubble debris heat up, effects of burn-up fuel, and so on, still showed limitations in MELCOR. For the fission product behavior, the comparison showed unexpected phenomena, various limitations, unresolved issues, and even absence of models. The issues summarized in this study have revealed the main areas where our endeavors need to be intensified in order to improve our understanding of severe accident phenomena.

From the analysis of the Phebus FPT-1 test results, not only new core damage features, such as foaming or core expansion, but also possible new fission product release patterns due to effects from a high burn-up fuel have raised alternative challenging phenomena that should be solved in the next severe accident research phase.

KEYWORDS : MELCOR, FPT-1, Core Damage, Fission Product, Aerosol, Iodine Chemistry, High Burn-up

1. INTRODUCTION

1.1 General Background

Since the TMI-2 accident in 1979, a worldwide effort has been undertaken to understand and model severe accident phenomena in nuclear reactors in hypothetical loss of core cooling accident. The aim of the Phebus FP experimental program is to study the core degradation phenomena and the behavior of the fission products (FP) in the reactor coolant system and containment building. Theresults and information obtained from this program will contribute to improving our knowledge and validating severe accident codes.

1.2 Purpose of the Study

The purpose of this paper is to draw out the new findings and confirmed results from the vast amounts of data from the Phebus FPT-1 experiment that concerns severe accidents and to report helpful information to MELCOR users to improve the use of the MELCOR code.

1.3 Description of the Experimental Facility

Figure 1 shows the nodalization of the Phebus FPT-1 experimental facility, consisting of five important components, for MELCOR. The first component is the reactor vessel and the core. The second is the vertical and horizontal pipes with a C point for simulating the hot leg in a real plant. The inside temperature of these pipes remains at 973 K over the transient.

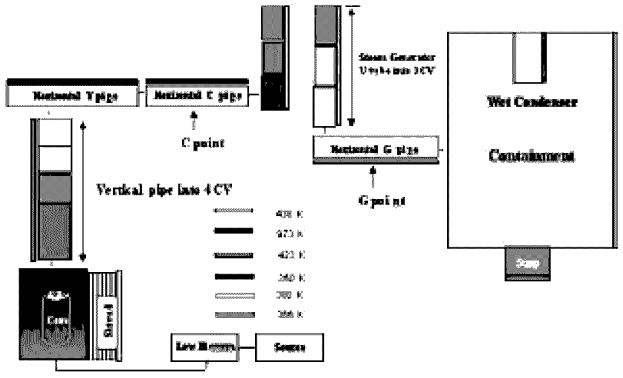

Fig. 1. Nodalization of the FPT-1 Test Facility for MELCOR

The third component is the steam generator (SG) U tube with 2 mm diameter. The fourth component is the cold horizontal pipe, with a G point, connected to the exit of the SG U tube. The inside temperature of the U tube and the cold horizontal pipe remains at 423 K over the transient temperature. The cold horizontal pipe represents the cold leg in the real plant. The last component is the cylindrical containment building, including the sump. The sump is included to simulate the cavity space beneath the containment building floor. The upper dome and bottom floor of the containment building are hemispherical.

Although the condenser does not exist in a real containment building, three condensers were installed in the upper dome of the simulated containment building. These three condensers simulate the condensing phenomena that occur on several cold surfaces that may exist in a steam-filled containment building under the condition of a severe accident.

1.4 Phases Included and Interesting Points

The overall experiment is divided into four important phases: core degradation, fission product transport/ deposition through the circuit, suspension of the aerosol behavior in the containment building after isolation from the circuit, and fission product chemistry within the sump pool.

The core damage was designed to progress by imposing a reactor power with an incremental increase method under a various amounts of steam injection. The core was kept in a dry condition with steam over a transient. The incremental power increase in the core aimed to produce the desired typical core damage scenarios, such as a slow core heat up, a fuel cladding rupture, pre-oxidation, oxidation shooting, candling, slumping, and fuel melting, under conditions similar to those in a severe accident. As the large loss of coolant accident progressed with a low pressure over the transient, only the low pressure was considered as a condition of the Phebus FP experiments.

The average level of a burn-up for the Phebus FP tests was distributed between 24 GWD/MTU and 32 GWD/MTU. In FPT-1, the 23 GWD/MTU burn-up rods were used. The Ag-In-Cd control rod was used for all tests, except FPT-3 with B_4C. The initial fission product inventories in the core could not be measured directly; therefore, they were estimated based on a calculation from a code such as PEPIN code [1].

The structure materials and fission products released from the core pass through the RCS (Reactor Coolant System). During their passage through the circuit, the chemical reactions between the structure materials and fission product, and the interactions with the walls were examined. The mass flow rates of the released fission products were measured at both the C point and G point, which are installed before and after the steam generator U tube, respectively. Using these two data, the mass balance was checked for each element.

In the SG U tube riser section where the inside wall temperature changed rapidly from 973 K to 423 K, the amount of deposition resulting from the large temperature gradient between the injected hot gas and the cold U tube wall was examined.

Before closing the connection valve between the circuit and containment building at the end of the core damage, the structure materials and fission products released from the core must accumulate within the containment building, excluding the deposit along the RCS. After the isolation, the deposition and physical behavior of the suspended aerosols in the containment building were studied. This is the aerosol phase of the test.

After the suspended aerosols settled completely, the bottom floor of the containment building was washed using a spray system. The washed water mixed with the deposited fission product was then transferred into the sump pool; there, the chemical behavior of the dissolved fission product under radiation and its volatility were examined.

1.5 Phebus FP Test Status

The Phebus FP program has been performed by IRSN (Institut de Radioprotection et de Sûreté nucléaire) in

Table 1. The Phebus FP Test Conditions and Testing Dates

	Fuel condition (burn-up)	Control rod	Objectives	Date
FPT-0	Fresh rod	Ag-In-Cd	Core damage & max FP release under a steam rich condition	1993
FPT-1	23 GWD/MTU	Ag-In-Cd	As FPT-0 but with irradiated fuel	1996
FPT-2	32 GWD/MTU	Ag-In-Cd	As FPT-1 but under a steam poor condition	2000
FPT-3	24 GWD/MTU	B4C	As FPT-2 but with a B4C effect	2004
FPT-4	38 GWD/MTU	N/A	Lower volatile FP release from rubble debris & up to molten	1999

France under the framework of an international cooperative research program, which also involved several partners including the EC, US-NRC, KAERI, JAERI, NUPEC, Canada, Switzerland, and Eastern european countries. Table 1 shows the experimental conditions, features, and dates of the Phebus FP tests.

1.6 Status of KAERI Participation and Application

KAERI has participated in the Phebus FP program since 1991. The Phebus FP experimental data have been applied to develop a modular code for severe accident phenomena and to validate MIDAS, which KAERI is developing as a database engine for the SARD system [2].

This paper presents a summary of the experimental results from the Phebus FPT-1 test and the lessons learned with MELCOR. The first section of this paper is concerned with the core damage and melt progression. The second section consists of the fission product release and its behavior both in the circuit and in the containment building. Finally, an overall summary is given.

2. RESULTS AND THE LESSONS LEARNED

2.1 Core Damage and Melt Progression

2.1.1 Early Phase of Core Damage

The early phase of core damage is defined as the time period before the initial core geometry begins to change.

2.1.1.1 Radiation Heat Transfer

In modeling the radiation heat transfer between the fuel rods in the core, there are no issues in the case of a relatively large sized core as in an actual plant, but there were some difficulties in simulating a small sized core, such as the core used in the Phebus FP test. Particularly, MELCOR had difficulties with the corner rods. The radiation model in MELCOR does not consider the configuration of each rod within the bundle, but simply imposes the user-defined average view factor value on each ring, which is a group of fuel rods within the same peripheral zone as defined by a user.

2.1.1.2 Ballooning and Rupture

In FPT-1, the inside of the fuel rod was pressurized to 23.6 bar with helium gas prior to the test. The circuit pressure was maintained at approximately 2 bar over the transient. From the FPT-1 results, it was confirmed that a fuel rod rupture depends on the temperature gradient along the periphery of the cladding (azimuthal direction) and the pressure difference. For all fuel rods in the core, the degree of the temperature gradient in the azimuthal direction can be categorized into two regions.

The first region was the central zone of the core, which has a relatively low temperature gradient. The second was the outer zone of the core where the temperature gradient was relatively large due to the large temperature difference between the outer core zone and the cold shroud. Therefore, rod ruptures in the outer zone occurred earlier than those in the central zone. This created the largest ballooning of the rod in the central zone of the core.

The degree of ballooning is estimated by the hoop strain, which is defined as the ratio of the original radius to the difference between the actual radius and the original radius. If the azimuthal temperature gradient is small, the hoop strain value will be large, and vice versa. In FPT-1, the average hoop strain of the ballooned cladding in the central zone was approximately 50 ~ 60% However, the average hoop strain at the outer zone was approximately 33%. The theoretical maximum hoop strain for the complete contact was estimated to be 70%. It is expected that ballooning may cause resistance to the fluid flow along the channel. Nevertheless, the experimental results showed that no pressure difference between the upper and lower sections of the ballooned location was detected under this condition. MELCOR does not have a model to simulate the ballooning phenomena. The issue that remains is the effects of the internal downward relocation of the particulate fuel debris through the ballooned region on the allowable peak cladding temperature using the ECCS criteria under the LOCA condition [3].

Usually, a fuel rod rupture occurs in the middle axial level at a cladding temperature of 1000 ~ 1100 K. MELCOR uses this threshold temperature value to impose the cladding rupture. The timing of a cladding rupture is predicted well at 1100K for the FPT-1 test. The issue that remains for fuel rod ruptures is the estimation and modeling of the burn-up effects on the cladding rupture phenomena.

2.1.1.3 Oxidation and Hydrogen Generation

The most important issues concerning the oxidation reaction are the peak hydrogen generation rate, the main production period, the final degree of total core oxidation, and the new oxidation correlations under special conditions such as oxidizing, reducing, and air.

From the FPT-1 test, the peak hydrogen generation rate was measured at 0.1 g/s (~ 60 C/min) and most of the hydrogen was generated during the rapid oxidation period (1853 ~ 2200 K). Approximately 55% of the total amount of hydrogen produced was generated during this rapid oxidation period. An additional hydrogen production period was the heat up phase, which aimed to produce a molten pool. In this period, approximately 17% of the total amount of hydrogen produced was generated. Also, approximately 20% of the hydrogen was generated during the pre-oxidation phase [4].

In the FPT-1 test, the final degree of oxidation for the core was determined by the mole ratio from the oxidation reaction based on the initial inventories for the three representative elements: zircaloy, steel, and ruthenium. The oxide forms for these elements were assumed as ZrO_2, Fe_2O_3, and RuO_4, respectively. From the FPT-1

results, the average core oxidation percentage was estimated to be 56% (64% based on only Zr mass). However, MELCOR, based on only the oxide form of Zr, predicted a core oxidation of approximately 65%.

The total H_2 generation mass predicted using the Urbanic correlation was 98 g, which was very close to the measured data of 96 g. The timing of the two oxidation peaks were also predicted well, but the Zr oxidation rate was slightly overestimated. Figure 2 shows the comparison of the hydrogen generation mass between MELCOR and the measured data over the FPT-1 transient.

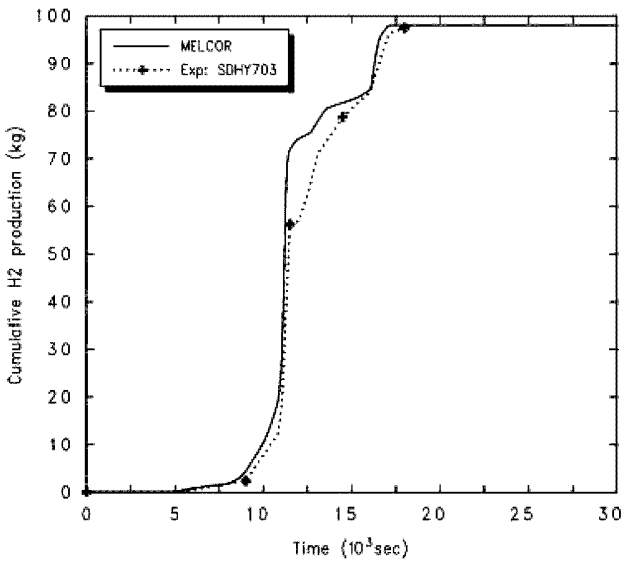

Fig. 2. Hydrogen Mass Produced in FPT-1

For the oxidation kinetics correlation, there are three available correlations: the Urbanic-Heidrick, Prater-Cathcart-Pawel, and Baker-Just correlations. The Prater-Cathcart-Pawel correlation is only valid until the early phase of the LOCA. The Baker-Just correlation over-predicted the oxidation reaction over the entire temperature range. These correlations were made based on either the oxide thickness or the total oxygen mass gain. The evolution of the bundle temperature, total amount of hydrogen produced, and the kinetic behavior of the oxidation reaction are reproduced well by MELCOR using the Urbanic-Heidrick correlation based on the total oxygen mass gain. Using a correlation based on the oxygen mass gain for MELCOR can be explained by the oxidation model limitations in MELCOR and based on the existence of only two layers: the pure zircaloy and the zircaloy oxide (ZrO_2).

The issues that remain for the oxidation phenomena are the validation of the MELCOR oxidation model under the air ingress condition and the steam starvation condition (FPT-2). The oxidation heat generation under the air condition is more violent than that of the steam condition. Thus, it is expected that the air oxidation phenomena may be accounted for in the case of a loss of cooling accident in the refueling storage tank and the failure of a lower vessel head. Furthermore, the validation of the B_4C oxidation model in FPT-3 is an important issue that remains because the methane produced from the oxidation of B_4C by steam can dissolve into the sump pool. Subsequently, this methane reacts with the iodine to form a volatile organic iodine (CH_3I).

2.1.1.4 Control Rod Failure

Based on the Phebus FPT-1 test results, the current understanding of the Ag-In-Cd control rod failure mechanism was reconfirmed. The type of control rod failure depends on the system pressure level. Under a low pressure condition like Phebus FPT-1, the failure of the cladding occurred at approximately 1400 K in a pinhole shape due to the eutectic reaction occurring at the contact point of the ballooned stainless steel cladding and the Zr guide tube. The failure temperature depends on the ballooning speed of the stainless steel cladding to make contact with the guide tube. In the case of a pinhole failure, the violent ejections of the molten absorber to the adjacent fuel rods accelerate the fuel rod degradation due to the eutectic reaction between the sprayed absorber and the zircaloy. In a high pressure condition, the cladding failure was delayed until the stainless steel cladding melted at 1700 K. In this case, most of the molten absorber relocated downward without a strong interaction with the neighboring rods. Although the control rod failure under a high pressure condition was not examined in the Phebus FP tests, the CORA test results showed the failure type as a benign mode.

The issues that remain are the modeling of the control rod failure mechanism, the release of the B_4C absorber, and the effect of boron on the fission product behaviors.

2.1.1.5 Oxide Layer Failure

When the cladding temperature reached the phase transition temperature from tetragonal to cubic at approximately 1853 K, the magnitude of the steam injection had a considerable effect on the temperature escalation gradient and the peak oxidation temperature. In the Phebus FPT-0 with a sufficient steam-supplied condition (steam injection rate = 3 g/s), the peak oxidation temperature was approximately 2773 K. However, in the FPT-1 with a medium level of steam injection (steam injection rate = 2.2 g/s), the peak oxidation temperature was approximately 2500 K [5]. In addition to the amount of steam injection, another parameter influencing the peak temperature and the amount of hydrogen mass produced was the timing of the oxide layer failure, which holds the molten zircaloy inside. The information for the above mentioned two parameters

concerning the oxide layer failure was not provided from FPT-1 test. The longer the oxide layer failure was delayed, the more the peak temperature and amount of hydrogen mass produced increased. From the Phebus FP results, the recommended values of these two parameters are an oxide temperature of 2600 ~ 2700 K and an oxide thickness of less than 250 μm, respectively.

MELCOR adopts the two above-mentioned parameters as the default criterion for an oxide layer failure. We applied a cladding temperature of 2400 ~ 2700 K and an oxide thickness of 10 mm to three Phebus FP experiments: FPT-0, FPT-1 and FPT-2. Although the values for the parameters showed a reasonable prediction for the temperature escalation and hydrogen mass produced, some fine-tuning was required for these two parameters to obtain a reasonable prediction. The issue that remains is the identification of a more fixable empirical value for the failure mechanism of the ZrO_2 layer.

Figure 3 shows the rapid temperature jump that results from the fuel material relocation into the lower level at 30 cm, as in the actual test.

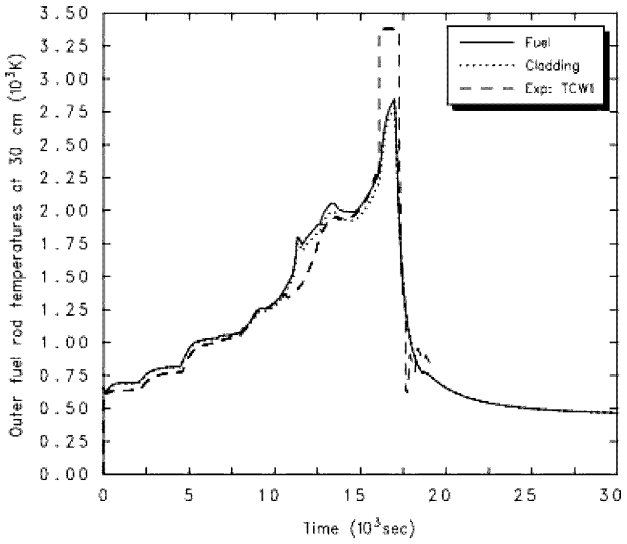

Fig. 3. Fuel Temperature at 30 cm in Ring 3

2.1.2 Late Phase of Core Damage

The late phase is defined as the time period after the initial core geometry has changed.

2.1.2.1 Eutectic Reaction

The special feature found in Phebus FPT-1 was the early liquefaction of the fuel and its relocation. In FPT-1, the fuel relocation was initiated at approximately 2100 ~ 2200 K. From the MELCOR model, it is expected that the fuel relocation can begin after the oxide layer fails at approximately 2500 ~ 2600 K. A possible reason for this early liquefaction and relocation may be explained by the eutectic reaction and the effect of a burn-up, such as a crack, swelling, or penetration, of the melt absorber into the cracks of the fuel.

The representative eutectic reactions occurred in three places during Phebus FPT-1. The first reaction occurred in the region where the cladding and the two grid spacers (Zr/Inconel) contact. This reaction can begin from approximately 1210 K. The second reaction occurred at approximately 1470 K between the cladding and the region where the ejected absorber was sprayed. Particularly, the eutectic reaction was accelerated within the ruptured cladding where the molten absorber material was sprayed. The final reaction occurred among the three components (UO_2/molten Zr/ZrO_2); for example, the outer surface of the fuel pellet and the inner surface of the oxide layer are dissolved simultaneously by the molten zircaloy. This reaction can begin after the pure zircaloy melts at 2038 K.

The dissolution of the solid UO_2 and ZrO_2 by the molten zircaloy can be simulated with two options in MELCOR. The first option is the parametric method where the amount of dissolution is controlled by the user input values based on the existing molten zircaloy mass. This method shows an ad-hoc solution. MELCOR under-predicted the dissolved UO_2 mass with the first option. The second option is a mechanistic method with a parabolic rate constant under the condition of selecting the eutectic option.

The key issue that remains for the eutectic reaction is a study concerning the effect of a burn-up on early fuel degradation. Other possible issues include the development of an appropriate enthalpy curve and the estimation of a solid temperature value for a mixture with new materials such as steel and boron.

2.1.2.2 Slumping and Molten Pool Formation

In FPT-1, the core slumping could not be predicted well by the default model in MELCOR using the pure UO_2 melting temperature of 3110 K. A good prediction for both the thermal behavior of the core and the final core damage state can be achieved by applying a temperature lower than the default to the threshold temperature value for fuel slumping. However, the cliff-edge effect due to the threshold value is the limitation for this model. A temporary remedy for this limitation could be to derive a conclusion from the results of a sensitivity study.

The early and progressive liquefaction of the fuel as it occurred in FPT-1 cannot be explained only by the use of a lower threshold temperature for the damaged core slumping. The reason for this early degradation of the fuel may be attributed to the interaction of an absorber material with the fuel, the unknown effect of iron, chrome, and nickel on the fuel dissolution within the melt corium, the effect of a fuel stoichiometry, and/or the effect of a

burn-up [6]. Therefore, the effects of the above-mentioned phenomena should be studied in more detail for a better understanding of the early core degradation mechanism.

In a severe accident, a molten pool can be formed by heating the rubble debris that has accumulated above the lower support plate, as in the TMI-2 accident. But in the FPT-1 test, the molten pool was formed above the lower grid spacer by a progressive accumulation of the materials from a upper part, such as slumped fuel debris, dissolved fuel and oxide zircaloy, molten zircaloy and the liquefied mixture of the absorber and the stainless steel by a chemical reaction.

From the post examination results of the FPT-1 test, the composition of the molten pool was revealed as considerably homogeneous and the atomic compositions for each of its constituents were $(U_{0.48}Zr_{0.48}Fe_{0.03}Cr_{0.01})O_{2\pm x}$. The melting temperature achieved was estimated to be 2760 K; this is in good agreement with the binary phase diagram of UO_2/ZrO_2. The mass of the molten pool depends on the accident scenario, but molten mass of 2 kg (1 kg from relocation and 1 kg from the melt in place) was produced in FPT-1 test. The peripheral crust thickness was measured to be 4.5 ~ 9 mm; however, the actual thickness may be lower than these values after taking into account the rapid cool down at the end of the test.

Concerning the corium relocation, the grid spacer played the role of catcher for the relocation of the molten corium at the core bottom.

2.1.3 Special Effects of a Burn-up Fuel

In the FPT-1 test with a burn-up fuel of 23 GWD/MTU, a fuel swelling and foaming occurred in the central zone of the core. This foaming phenomenon began at 2300 K and it lead to a decrease in the radial heat transfer to the shroud. This decrease caused the fuel temperature in the inner region to increase rapidly and the foaming resulting from the fuel melt can produce a flow blockage.

This swelling and foaming causes the bundle to expand to the shroud. These phenomena could induce a vessel attack or a complete flow blockage of the core. These new features from the burn-up fuel found in the FPT-1 test raised alternative challenging phenomena for the following severe accident research phase. Using a cross-sectional view of a damaged pellet, Fig. 4 shows the difference in the fuel porosity between a fresh fuel rod and an irradiated one from the FPT-1 test.

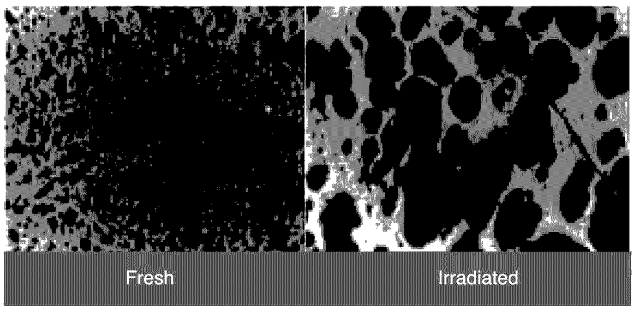

Fig. 4. Difference Between a Fresh Rod and a Burn-up Rod Using a Cross-sectional View of a Damaged Pellet from the FPT-1 Test

2.1.4 Overall Progress of Core Damage in FPT-1

The overall progress of the core damage from the Phebus FPT-1 test can be summarized as follows:

- fuel cladding rupture
- control rod failure
- rapid oxidation,
- metallic blockage formation at the bottom level due to the relocation of partially dissolved cladding mixed with the sprayed molten absorber,
- slumping of the partially liquefied fuel pellet by the molten zircaloy mixed with the absorber material into the low level and freezing,
- heating of the slumped layer and forming the molten pool,
- subsequent molten pool movement to the lower level due to its weight and high temperature,
- end of the experiment.

2.1.5 End State Picture of the Damaged Core

In the upper region of the core, most of the fuel rod remained, but it had a high porosity due to dissolution by the molten Zr. In the middle region (between the two grid spacers), most of the area was void, except the peripheral zone which bowed due to the early and progressive liquefaction. In the lower region, most of the area was void, but a thick crust remained in the periphery due to the movement of the molten pool. Just under the lower region, a homogeneous thick layer was formed composed mainly of uranium. In the bottom region, most of the fuel rod was intact, and it was not completely oxidized. Consequently, the general schematic view of the end of the core damage produced by Phebus FPT-1 showed similarities to that of TMI-2. Table 2 shows the representative parameters concerning the core damage in three Phebus FP tests.

2.2 Fission Product Behaviour

2.2.1 FP RELEASE FROM CORE

2.2.1.1 Indirect Prediction of a Bundle Release

The experimental data for the FP release from the core was obtained at the circuit using an online gamma spectrometry and sampling with a bulb at discrete times. The measurement was performed at both before (C point) and after (G point) the SG U tube. The on-line aerosol measurement (OLAM) system gives qualitative information about the aerosol release.

The vertical and horizontal lines above the core exit

Table 2. Parameters Concerning Core Damage in Three Phebus FP Tests

Parameter / core damage / Test	T_{RUP} [K]	$T_{CR\,fail}$ [K]	Oxidation [%] IC	T_{melt} [K]	W_{pool} [w/o] Based on molten pool mass			
FPT-0	1100	1350~1723	64.9	2720	62.4	22.1	14.4	2.6
FPT-1	1118	1370~1700	64	2760	59.6	24.3	16.0	2.03
FPT-2	1073	1223~1698	84	NY	NY	NY	NY	2.4

* T_{RUP} : temperature of cladding rupture *$T_{CR\,fail}$: temperature of control rod failure
* Oxidation : oxidation % based on Zr inventory in the core * T_{melt} : corium melting temperature
* W_{pool} : weight fraction for U (uranium), Zr (zircaloy), O (oxygen) within the pool based on the pool mass
* M_T : total pool mass * NY : not yet analyized * IC : initial cladding mass

were designed to prevent the condensation of fission product vapors on the inner surface by heating the inner surface using an immersed heater. However, many of the released fission products were deposited to the core, including the surrounding vessel wall and upper plenum at the core exit in the Phebus FP tests. Therefore, a prediction of the amount of fission product released from the core based on the measured data at the C point requires a reasonable prediction of the deposition profile from the bundle to the C point in a horizontal pipe.

2.2.1.2 Overall Release Pattern

The overall release patterns of all the fission products, control rod materials, and structure materials in the Phebus FPT-1 test showed similar trends to the three peaks at the separate phases: the Zr oxidation, the fuel liquefaction, and the relocation of the molten corium, respectively. This implies that the generated aerosol can consist of all of the different elements released from the bundle. The only exceptions to these trends were Zr and Re, which had delayed releases.

A minor release from the ruptured cladding (FPT-1 ~ 1118 K) preceded the three above-mentioned peaks and it was characterized by the detection of Xe and Sb (the activation product of Sn) in the containment building. The Phebus FPT-1 did not provide data on the gap inventory when the cladding ruptures. Also, MELCOR does not have a model to predict the gap inventories. However, from a severe accident point of view, it appears that the exact modeling of the gap inventory is not as important as that of the cladding rupture itself.

2.2.1.3 Influencing Parameters on the FP Release

The Phebus FPT-1 test implies that the fission product release depends on the degree of burn-up, the fuel temperature, the temperature increase rate, the duration of a temperature plateau, the pellet radial temperature gradient, the partial pressure of the steam, the deviation of the fuel stoichiometry, the bundle degradation features (dissolution, oxidation, damaged geometrical shape, etc.), the ratio of oxygen to hydrogen in the transporting fluid, and the chemical interactions with other materials.

2.2.1.3.1 Effects of Fuel Stoichiometry

The fuel stoichiometry (ratio of metal to oxygen) can be increased either by an extended burn-up or by oxidation. Also, a variation in the temperature across the fuel section can establish a deviation in the stoichiometry. This deviation can increase the fission product mobility. Moreover, the cracking that results from the fuel expansion can increase the stoichiometry by extending the contact surface with the steam. Generally, even a small increase in the stoichiometry can increase the release of the fission product. But it is also known that the release of low and semi-volatile elements, such as Ba and Ru, are less sensitive to fuel stoichiometry.

Although it has uncertainty, the post examination result from FPT-1 in the middle core region showed a super stoichiometry of ~ 2.11. There are many different forms of oxide fuels that can be formed at specific temperatures and pressure conditions, such as U_3O_8, UO_{2+x}, and UO_3. Especially, U_3O_8 is formed under a condition of both a high temperature and a high steam pressure, making the vapor diffusion easy and expanding the fuel volume. In MELCOR, the parameters that consider the effects of stoichiometry are the effective grain size and the diffusion coefficient within the grain for the CORSOR-Booth model.

2.2.1.3.2 Transport Fluid Composition Effect

The comparison of the release characteristics for each element from FPT-1 between the pre-oxidation phase (oxidizing environment) and the rapid oxidation phase (reducing environment) showed that the releases of Te and Ru were favored under an oxidizing condition (low H/O ratio: early oxidation phase); whereas the releases of Ba, Sr, and Cd were favored under a reducing condition

(high H/O ratio: late oxidation phase). However, the release of Cs, Ag, In, Sn, and I was not affected by the mole ratio of oxygen to hydrogen in the fluid. MELCOR does not have a model to simulate the thermo-chemical equilibrium in the RCS.

2.2.1.3.3 Effect of Interactions with Other Materials

An example concerning the interaction of the fission product with other materials can be found in the release data of Mo from the FPT-1. Generally, interactions with other materials can have a great influence on the release of low-volatile elements, but not volatile elements. From the FPT-1 test, MELCOR predicts a Mo release of 17% based on the initial core inventory. However, Mo, a less volatile element, had a significant release of 56% as was measured in the FPT-1 test. The reason for this high release of Mo may be attributed to the interaction of Mo with Cs and other fission product elements. Therefore, the dominant compound form of Mo should be identified. From the recent SNL study with MELCOR for the FPT-1 test, the dominant compound form of Mo is Cs_2MoO_4 [7].

2.2.1.3.4 Effect of a Chemical Reaction

The eutectic reaction between the fuel and cladding material can enhance the release amount and make the release time earlier for a volatile fission product. On the contrary, it can also limit the amount of release and retardate the release for less or non-volatile fission products such as Zr and Re. The out of pile experiments, such as VI and VERCORS, showed that 30 ~ 80 % of Ba was released under similar conditions to that of Phebus FPT-1; but the FPT-1 test showed the release of Ba at less than 5%. The reason for this very low Ba release in the FPT-1 test is explained either by the eutectic interaction between the fuel and Zr (or stainless steel) or by the short plateau at the peak temperature. This interaction causes the vapor pressure of Ba to decrease by forming barium zirconate. In FPT-1, Ba was released during the rapid oxidation and molten pool phases.

2.2.1.4 Volatile Fission Product Release

The Phebus FPT-1 results showed a very high release of 80 ~ 100% for volatile elements such as I, Cs, and Te. MELCOR accurately predicted the total amount of release for the volatile elements (~ 80%), as well as noble gas. But the release rate during the period of rapid oxidation showed an excess prediction with MELCOR. This may occur because the CORSOR type model only considers the effect of the fuel temperature. However, Phebus FPT-1 implies that a good prediction of a volatile fission product release from the fuel could be obtained by considering the effect of the fuel temperature escalation rate and fuel state.

Furthermore, a comparison of the calculation results from multiple organizations in the international standard problem N° 46 for the Phebus FPT-1 test showed that various codes predicted a similar amount of release at 80 ~ 100% for volatile elements [8]. This implies that the current release models for volatile FP release have a high level of consensus. But an uncertainty about the release model for iodine remains because its chemical form and physical state (vapor or aerosol) during the release has not been clearly identified yet.

2.2.1.5 Low- and Semi-Volatile FP Release

It is known that the semi-volatile elements are Te, Ru, Mo, Sn, and Ag. These elements have a tendency to be non-volatile in a moderate temperature range, but they become volatile in a high temperature range. Also, it is known that Ba, Sr, Zr, and U belong to the low-volatile elements. Normally, these non-volatile elements are not released from a fuel, except during fuel vaporization.

From the FPT-1 test, the semi-volatile Mo was released at 56%, but the release of a low-volatile element such as Ba was only 5%. The results of ISP-46 for FPT-1 showed a wide dispersion of the predicted values, from a few percent to 60%, by the various codes on the low- and semi-volatile elements. This wide dispersion shows that there is no general consensus on a model concerning the low- and semi-volatile elements.

It is necessary that the release model for the low- and semi-volatile elements be improved and validated by considering the state of the core damage and the chemical interactions with other materials. The MELCOR calculation for FPT-1 showed a general trend that the lesser volatile elements, such as Mo, are under-predicted and the low-volatile elements, such as Ba, are over-predicted.

2.2.1.6 Absorber Materials Release

Regarding the release of the Ag-In-Cd absorber material, the release of Cd and In was important during the early stages of the oxidation phase. Whereas the Ag release was important during the late stages of the oxidation phase when the molten corium relocates downward to the bottom level, where the frozen silver is accumulated.

In the FPT-0 test, indium was transported in a vapor state through the horizontal pipe at 973 K. However, the FPT-1 result showed that most of the In was transported in an aerosol state through the horizontal pipe at 973 K. The differing states of In at 973 K in the two tests raises other issues that should be resolved. On the contrary, Cd was always measured in a vapor state at the C point in both tests. MELCOR assumes that both the elements of In and Ag are in the same group with a lower volatility.

Therefore, the treatment of indium in the same group as Ag must be verified. Moreover, MELCOR does not treat the release of Ag, In, and Cd as an absorber material release, but a fission product release within the core. Therefore, it is necessary that not only an Ag-In-Cd control rod failure model, but also an absorber release model be developed.

2.2.1.7 Release from the Molten Pool

Another astonishing result was the lower release rate of low-volatile elements, such as Ru, Ba, and La, during the molten pool phase. Until now, we have considered that all fission products can be released more easily in a molten pool state; however, the data measured in the FPT-1 showed that the total amount of release for the low-volatile elements was less than 3%. The reason for the lower release of low-volatile elements during the formation of a molten pool may be explained by both the decreased surface to volume ratio for a fission product gas escape and the formation of a stable material using the low-volatile elements within the pool.

MELCOR over-predicted the release of Ba with a low volatility at 30% when compared with the measured value of approximately 5%. The primary reason for this over-prediction of the total amount of Ba release was due to the over-prediction of a release during the molten pool phase. It is necessary that the Ba release coefficient of CORSOR over 2200 K be evaluated against other test data.

Figure 5 shows a comparison of the released amounts of FP between the measured data and the calculated results using the three representative release models, CORSOR, CORSOR-M, and CORSOR-Booth, in MELCOR. CORSOR -M predicted the total amount of FP release from the core better than the other models. Also, the CORSOR-Booth model showed a tendency to under-predict the total FP release amount for all fission product elements.

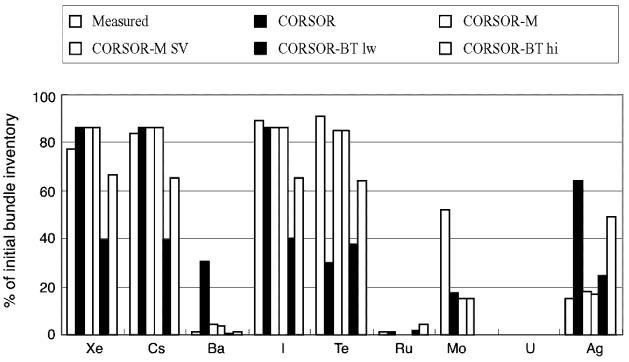

Fig. 5. Comparison of FP Release Percentages between the Measured Data and the Results from the Three Models in MELCOR

2.2.2 Transport and Deposition in RCS

2.2.2.1 Chemical Form of Iodine During Transport

The fission products released from the fuel were transported through the circuit to the containment building by the force of the steam injection flow mixed with the produced hydrogen gas. During the transportation, the circuit (the vertical and horizontal lines for the hot leg at 973 K) can be considered as a reaction chamber where various elements are reacting. Consequently, the circuit is similar to a chemical reaction chamber. The important issue during the transportation is the dominant chemical form of iodine, its physical and chemical state, and the volatility of its compound.

Regarding the physical state of iodine in the FPT-1 test at 973 K, all of the iodine at the C point was transported in a vapor state. Thereafter, most of the vapor-state iodine was condensed and deposit in the SG U tube riser where the gas temperature changes abruptly from 973 K to 423 K. Most of the iodine flowed in aerosol form from the cold horizontal line (G point), but an unknown fraction of iodine (2% of the total iodine aerosol mass at the G point in the FPT-0 test) was detected in a vapor state at 423 K. Iodine's form in the circuit can be I_2, CsI, or AgI. MELCOR allows the user to define the iodine compound form during the transportation: it can be CsI or AgI. The issue that remains is the identification of the existing gaseous or vapor form of iodine in the circuit.

2.2.2.2 Importance of the Bundle Deposition

The released fission products can be deposited by vapor condensation over the core region. The deposition depends on the temperature profile of the bundle and the location of the cold region that occurs from the formation of a flow blockage. Particularly, in the Phebus FPT-0 test results, Ru was released significantly during the molten pool phase, but most of the released Ru was deposited within the core region by condensation at 1600 K. Consequently, although the Ru was released, the amount of released Ru was lower than the estimation of 1 ~ 4%. The important detail in terms of the source is that the Ru deposit over the core has a possibility for revaporization by oxidation with the ingress air in a bottom head vessel failure. Furthermore, it is known that the toxic level of Ru is similar to that of iodine; therefore, the amount of Ru deposit within the bundle should be accounted for in the source term calculation.

2.2.2.3 Location of the Main Deposition

The two main locations where a large deposit occurred were the upper plenum and the vertical line, the SG U tube riser where the wall temperature changes abruptly from 973 K to 423 K. The deposition of all fission products (except I and Cd) in the upper plenum and the vertical line appears to occur due to vapor condensation and an unknown deposit mechanism. The deposition in the riser seems to occur primarily due to the thermo-phoresis phenomena.

The MELCOR calculation also showed the same large deposit areas as that of FPT-1. Figure 6 shows the distribution of the FP deposit amounts along the circuit. However, from the point of view of the deposit amount, MELCOR under-predicted the section of the upper plenum and the vertical line, and over-predicted for the SG U tube riser.

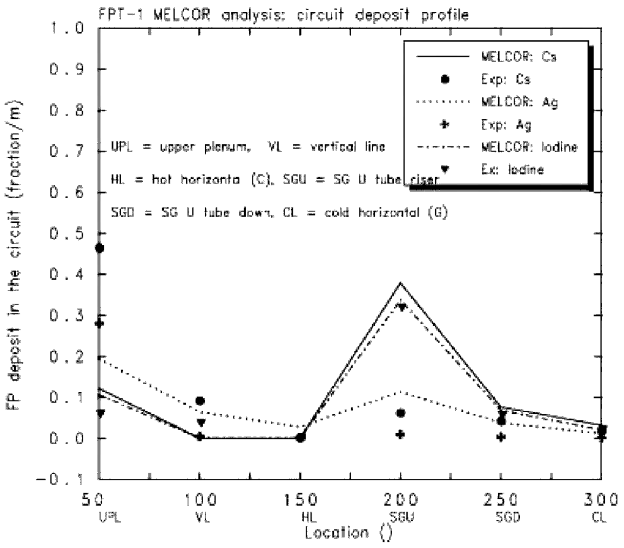

Fig. 6. Distribution of FP Deposits Along the Circuit

2.2.2.3.1 Deposition on the Upper Plenum and Vertical Line

First of all, for the deposition over the upper plenum and vertical line, the heating of the inside surface of the upper plenum and vertical line to 973 K aimed to prevent condensation of the flowing vapor occurring. However, a reasonable explanation for the occurrence of a large deposition in this area is still not clear. A possible explanation for the occurrence of this deposition may be explained by considering the existence of an unheated section just after the exit of the core, a vapor condensation, and unknown deposition phenomena.

In addition to the occurrence of the deposition itself, we need to solve the problem of the under-prediction of the deposition amount on this section. Therefore, it is necessary that the phenomena concerning the vapor condensation and deposition occurring on a structure surface at a higher temperature than its saturation temperature be studied.

There are two important factors concerning the condensation of vapor in MELCOR. The first factor is the mass transfer coefficient of the fission product vapor of interest to a wall or an aerosol surface. This mass transfer coefficient is determined using the Chapman-Enskog formula for the binary diffusivity of an FP vapor in a bulk gas. This diffusivity value can be calculated based on the Lennard-Jones parameter values for each FP element. However, the problem is that all FP elements, except Xe and I, use the value of air as their default.

The second important factor is the saturation concentration of an FP vapor on the surface based on the surface temperature. However, this saturation concentration can be calculated using the value of each element's vapor pressure. In MELCOR, the correlations of the vapor pressure for all representative FP elements are provided, including CsI. But it is necessary that a vapor pressure correlation on other FP elements, such as AgI and CH_3I, be implemented.

2.2.2.3.2 Deposition on an SG U Tube

For the deposition of FP on the SG U tube using the FPT-1 data, iodine showed the largest deposition fraction of 17% on the SG U tube riser section. But MELCOR over-predicted the deposition amount in the SG U tube riser section. Figure 7 shows a deposit mass comparison between MELCOR and the measured data along the SG U tube riser section under the same boundary conditions as those of the FPT-1 test.

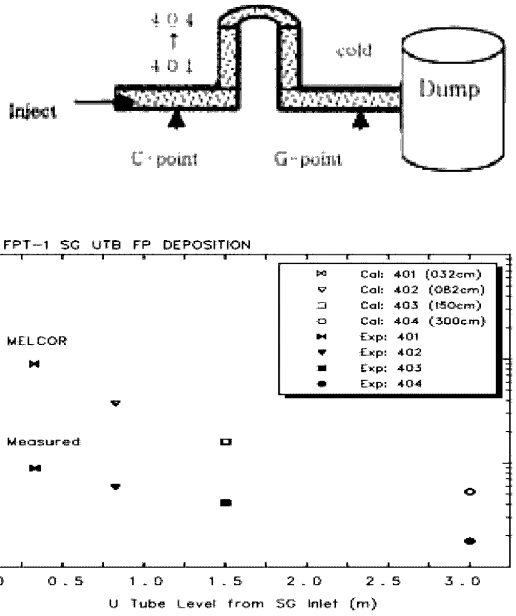

Fig. 7. Comparison of Te-129 Deposit Profile along the SG U Tube Riser Section (401-404) between MELCOR and the Measured Data

It appears that the thermo-phoresis force due to the large temperature gradient dominates the deposition phenomena in the SG U tube region. However, the current MELCOR model neglects the effect of the boundary layer developed near the inside surface of the pipe on the FP deposit by the thermo-phoresis phenomena. Therefore, the temperature and velocity profile within the boundary layer is considered under the condition of turbulence [9], but the resuspension phenomena were neglected.

Figure 8 shows the particle trajectories from the one-dimensional thermo-phoresis model where the effect of the boundary layer was considered. Although this model showed a considerable improvement in the over-prediction problem, other possible factors that could influence the deposit phenomena remain.

Other possible factors include the model parameters in the thermo-phoresis correlation, the insulation effect of the deposition, the thermally undeveloped flow condition, the surface roughness, other types of thermo-phoresis model, the effect of a non-spherical particle shape, and resuspension by a fast flow from the inlet of the SG. Consequently, it is expected that questions about the over-prediction in the SG U tube riser section can be answered by studying these possible factors.

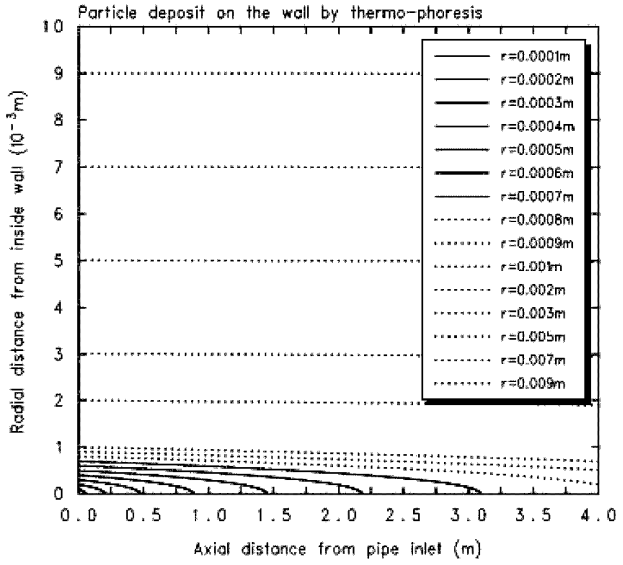

Fig. 8. Predicted Particle Trajectories from the One-Dimensional Model

2.2.2.3.3 Resuspension

Although the mechanical resuspension model has not yet been adopted by most of the severe accident codes, the resuspension of Cs was observed at the end of the core damage stage in the FPT-1 test. This indicates that resuspension has a potential effect on the evaluation of the source terms. The post-test analysis of the SG U tube showed that the deposited aerosols were loosely adhered to the inside surface of the wall. It is expected that the reflooding or relocation of molten material into the water pool can cause the resuspension phenomena. If resuspension occurs, then it will affect the shape of the deposition profile along the circuit and the concentration of an aerosol or vapor in the containment area. Therefore, it is necessary to implement the resuspension model for Cs in MELCOR.

2.2.2.4 Overall FP Mass Distribution in RCS

From the Phebus FPT-1 results, the overall characteristics of the deposition distribution over the circuit can be summarized according to their volatility, as follows.

The volatile elements such as iodine, cesium, and tellurium of 10~20%, except Mo at 40%, remain in the core at the end of a transient phase. Furthermore, the volatile elements from 15 to 38%, except iodine in a vapor state, were deposited in the upper plenum. The integral mass of the transported volatile elements at the C point was distributed between 30% and 60%. The deposit mass on the SG U tube for the volatile elements, except iodine, was 10%. The deposition amount for the iodine vapor showed 17% and it was the largest deposition element in the SG U tube.

Table 3. Distribution of FP Deposit (Percentage) from the Phebus FPT-1 Test

location / species	Core (1000 K<)	UPL+VL (973K)	Hz (hot) (973 K)	SG U-tube (423 K)	Hz (cold) (423 K)	Amount Containment Injection
I	13	5.3	0.2	19.2	0.7	64.1
Cs	16	25.7	3.1	10.7	0.6	43.8
Te	17	26	1.7	9.1	0.7	52.5
Mo	44	22	NE	6.8	0.5	23
Ru	99	0.59	NE	0.09	NE	0.5
Ba	99	0.27	NE	0.12	NE	0.65
U	99.86	NE	NE	0.021	NE	0.119
Ag	85	7.5	NE	0.9	0.1	6.7
In	91	NE	NE	1.2	0.01	7.8
Cd	33	NE	NE	15.2	0.8	10.4

*NE : could not evaluated due to small mass or technical problem

More than 90% of the less volatile elements, such as barium and ruthenium, and the low-volatile elements, such as uranium and zircaloy, remained within the core at the end of the transient phase. Also, the lesser volatile elements were deposited on the upper plenum at lower than 0.5%.

More than 80% of the absorber materials, such as indium and silver, remained within the core; but the cadmium vapor remained at approximately only 30% within the core at the end of the transient phase. Approximately 10% of the silver released was deposited in the upper plenum region; but In and Cd were not deposited in this region because they were in a vapor state. The integral mass of the transported indium and silver at the C point was less than 10%, but the cadmium was released in a vapor state. Table 3 shows the distribution of the FP deposit percentages based on the initial core inventory for the Phebus FPT-1 circuit.

2.2.3 Aerosol Behavior in the Containment

2.2.3.1 Aerosol Size and Distribution

To accurately predict the aerosol behavior in the containment building, it is necessary to have information such as the particle shape, composition, and corresponding number of particles versus their diameter. However, first of all, the information regarding the aerosol size is the most important to model the aerosol behavior in the containment area. The size of the aerosol was measured at three locations, the C point, G point, and in the containment area, using an impactor and a sampling bulb. The data from the six-stage impactor was used to determine the aerodynamic mass mean diameter (AMMD) [10].

From the FPT-1 test, the measured data at the C point (hot leg) showed that the AMMD and standard deviation were 1.5 ~ 2.0 μm and 2.0, respectively. However, the aerosol mass distribution at the hot leg could not be described as a lognormal distribution. This may be because the distribution was multi-modal, which shows a superposition of a multi-population of aerosol due to complex processes in the hot leg circuit such as an agglomeration or condensation. But the results from the G point (cold leg), which were 3.0 μm and 2.0, respectively, showed a lognormal distribution. The results from the containment area also showed a lognormal type with an AMMD of 3.5 ~ 4.0 μm and a standard deviation of 2.0. Consequently, these increases of AMMD along the circuit mean that fine particles agglomerated to form a larger sized particle as they moved from the circuit to the containment building.

From the lognormal distribution function of the mass fraction versus the diameter at a specified time and the G point using MELCOR, the AMMD was predicted to be half of the measured data. But the predicted increase of AMMD through agglomeration in the circuit was similar to that of the measured data. From the calculation results with MELCOR in the FPT-1 test, the agglomeration trend was predicted well, but it depended on the aerosol density and diameter.

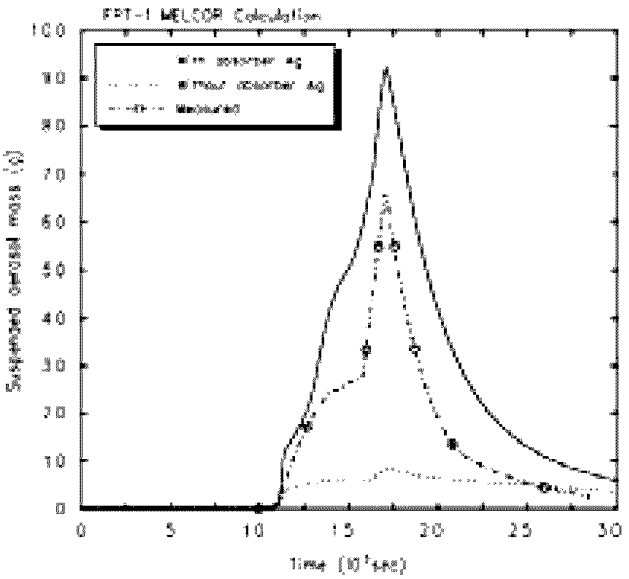

Fig. 9. Change in the Suspended Aerosol Mass vs. the Amount of Ag Release

Figure 9 shows the effect of increasing the amount of silver released on the suspended aerosol mass and its depletion rate. The FPT-1 test showed a maximum aerosol density of 7 g/m^3 in the containment area and it appears to be a representative value in severe accident conditions.

2.2.3.2 Inner Composition of an Aerosol Particle

The trapped aerosol particles consist of multiple components and the elemental weight compositions were homogeneous and independent of their aerosol size. During the zircaloy oxidation phase, the major elements within the aerosols were primary Ag and other absorber materials such as In, Cd, and steel.

However, as the core degradation phase neared the end, in addition to Ag and Re, U and Cs became major elements of the aerosols in the containment area. Specifically, it was found that Cs was included in a small fine particle form within the aerosol. These findings contributed to the simplification of the nucleation model of an aerosol in SCDAP/RELAP5 [11] by considering the seed material as Ag and U. The simplified nucleation model can be applied successfully after considering the other elements only as condensing materials over the seed element. From the calculated result from MELCOR in the FPT-1 test, the deposited material on the bottom floor of the containment building consisted of Ag, Cs, and U in order of their existing masses within the particle. The experimental data also showed a similar order for Ag, U, Cs, and Te.

2.2.3.3 Solubility of Aerosols

The information regarding the solubility of each element is important to predict the gravitational settling of the aerosol due to the steam condensation over the aerosol surface resulting from the hygroscopic phenomena. In MELCOR, the dissolved aerosol's chemical activity in the condensed water was determined by the van't Hoff correlation, which models CsOH and CsI as the only soluble elements. But essentially, whether the hygroscopic phenomena should be considered or not depends on the possibility of the existence of a very high soluble material in the aerosol and the location of a soluble layer in the multi-deposit layers over the aerosol. If a soluble layer exists inside the porous aerosol, the condensation cannot affect the increase of the diameter, but it can affect the density of the aerosol [12].

The non-soluble elements are I, Te, Sb, La, Ru, Ag, In, U, Sn, and Pb. The partially water-soluble elements are Ba, Cd, Mo, Tc, and Re. The only fully water-soluble element is Cs. However, the Phebus FPT-1 test results showed that the solubility of the deposit aerosol inside the containment area increased after the oxidation of the aerosol in a steam rich atmosphere. For example, Re was transformed into the more soluble material Re_2O_7 by the oxidation reaction. The Cd and Ba metals were also transformed into soluble oxides or hydroxides.

2.2.3.4 Depletion of Suspended Aerosols

There were three types of deposition mechanism in the containment atmosphere over the transient. The first mechanism was the settling of the suspended aerosol particles over the bottom surface of the containment due to gravitational force. The second was the diffusio-phoresis on the wet condenser resulting from steam condensation and thermo-phoresis. The last mechanism was the deposition on the heated wall or the ceiling by an inertia force, such as an impact.

After isolating the containment from the circuit in the FPT-1 test, the suspended aerosol in the containment area decreased quickly and most of the suspended aerosol (~ 70%) was deposited on structures in the containment building within one hour. Within four hours, 99% of the suspended aerosol in the containment area was removed.

The Phebus FPT-1 results showed that a gravitational settling was the dominant mechanism for the removal of the aerosol masses in the containment area in a severe accident condition. The second mechanism was a condensation on the condenser by a diffusio-phoresis process. Approximately 70% of the total deposit mass was caused by gravitational settling and another 30% occurred by the condensation. Therefore, an accurate prediction for the agglomeration and condensation is very important to obtain reliable results concerning the suspended and removed aerosol masses in the containment area.

After the isolation of the containment area from the circuit, for all elements except Cs, the overall kinetics of the aerosol deposition process can be described with a decreasing process of the first order. The resulting time constant for removing the suspended aerosol was estimated to be 1.35 hours. But before the isolation, the time constant for the aerosol removal for all elements was estimated to be 0.65 hours, but Cs showed 0.9 hours. Therefore, it is necessary for a more detailed study concerning the difference of the deposition behaviors for Cs compared with other FP elements over the transient to be performed.

2.2.3.5 Condensation of Aerosols on a Wet Surface

In MELCOR, the mass transfer coefficient for the condensation models used the Sherwood number based on the heat and mass transfer analogy. The film thickness on the condensing surface can be either specified by user inputs (maximum 5×10^{-4} m) or calculated by the code, but only for interconnected structure surfaces where the film tracking option is selected.

The FPT-1 results showed that the amount of elements remaining on the wet painted surface depends on their solubility in the water in the film. Therefore, the deposit mass of soluble or partially soluble elements, such as Cs and Ba, on the wet painted surface was small when compared tothe other elements because most of the soluble elements dissolved into the condensate water, which is continuously drained into the sump.

MELCOR assumes that the deposited aerosol or condensed vapor on the surface is relocated together with the condensate water. The amount of relocated fission product mass is determined in proportion to the fraction of film that was drained. Although this needs fine-tuning for the solubility of each element in the water film, the calculation results in the FPT-1 test showed a good prediction for the masses deposited on the condenser and the masses transported to the sump.

2.2.4 Iodine Chemistry

2.2.4.1 Importance of Gaseous Iodine

Most of the FP aerosols injected into the containment building can be removed from the containment atmosphere by gravitational settling, deposition to the wall surface, and operation of the spray system. Normally in a severe accident, all suspended aerosols in the containment area can be removed naturally within a few days. However, the suspended gaseous forms of fission products, especially gaseous iodine compounds such as CH_3I and I_2, cannot be removed effectively by a spray or natural mechanisms. Even the charcoal filter cannot successfully remove the gaseous iodine. To remove this gaseous form of iodine, a special charcoal filter coated with TEDA (triethylenediamine) is required. However, this filter has a significant weakness in continuous operation due to the decay heat generation and the high level of humidity in a severe accident. Consequently, this suspended gaseous iodine may leak without

filtering. Therefore, it is expected that a study (iodine accident management) to minimize the suspended gaseous iodine concentration in the containment atmosphere is important for public safety.

2.2.4.2 Balance of the Gaseous Iodine in the Containment Building

After isolation from the circuit, the concentration of the suspended gaseous iodine in the containment area depends on the balance among three processes. These three processes are 1) the generation of organic iodine from the painted surface in the containment atmosphere; 2) the overall depletion processes in the containment atmosphere and sump; and 3) the generation and release of gaseous iodine from the pool to the atmosphere by partitioning. In addition to these three processes, the concentration of gaseous iodine in the containment area also depends on the amount of gaseous iodine entering the containment area directly from the circuit.

The depletion processes in the containment area are the deposition, settling, and destruction by radiation. These depletion processes proceed rapidly and massively in the early phase. After the complex chemical reactions in both the atmosphere and the pool in the late phase, the gaseous iodine concentration in the containment area reaches an equilibrium level by the balance between generation and destruction.

2.2.4.3 Source of Gaseous Iodine in the Containment Building

The gaseous iodine can be produced by either the organic materials dissolved in the pool or the painted surfaces in the gas phase. But among these sources, the painted surface has been identified as the main source of the organic iodine formation in the FPT-1 test. MELCOR assumes that the methyl iodide (CH_3I) or elemental iodine (I_2) can be partitioned to the containment atmosphere from the pool.

However, the current MELCOR (version 1.8.5) does not include any equations concerning the formation of organic iodine within the pool. Therefore, these equations were implemented into the pool chemistry model in MELCOR. The updated MELCOR can show the generation of organic iodine from the pool. However, Fig. 10 shows a large difference in the gaseous iodine concentration versus time for the three different cases. The first case is the calculation results with the iodine pool model in MELCOR, but this did not use the organic iodine generation model. The second case is the calculation results with the iodine pool model and the organic iodine generation model. The last case is the calculation results with MELCOR without using either the pool chemistry or an organic model.

The Phebus FPT-1 results show that the organic iodine can be formed not only from the pool, but also from the painted surface [13]. But MELCOR (version 1.8.5) does not include a model for generating organic iodine from the painted surface through the reaction of the deposited molecular iodine with the ketones or alcohol from the paint. In MELCOR, the issue that remains is the updating of the iodine pool chemistry model with recent data concerning the organic iodine generation, such as Phebus FP.

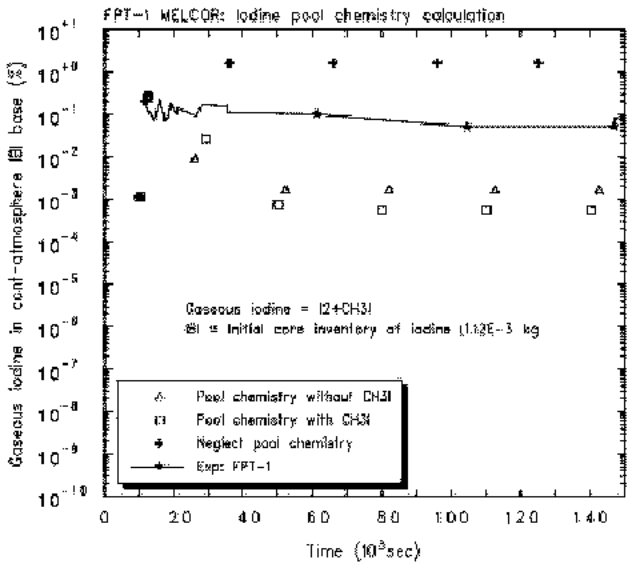

Fig. 10. Concentration of Gaseous Iodine in the Containment for the Three Different Cases

2.2.4.4 Influencing Factors for Gaseous Iodine

The most influencing factor on the formation of volatile iodine within the pool is the pH value of the pool. It has been shown experimentally that volatile iodine can exist more easily in the containment atmosphere when the pool remains in an alkali state. From the FPT-1 data, after washing, the pool acidification increased further. The Re_2O_7 and NO_X decrease the pH value of the water in the sump. However, the dominant elements for this acidification are still uncertain. In MELCOR, there are two sources for an acidification of the sump pool: hydrochloric acid from a cable and nitric acid from air.

Other factors that influence the concentration of gaseous iodine in the containment are the levels of radiation in both the gas and the pool, the mass of the cable, and the iodine concentration. In fact, it is difficult to clearly and properly define the values for the three above-mentioned parameters as input data.

2.2.4.5 Iodine Trapping within the Pool by Silver

An important finding in the iodine chemistry was the identification of the effect concerning the trapping of the iodine by silver within the sump pool. Silver iodide (AgI) can be formed by the reaction of the molecular iodine and

the iodine ion produced by radiolysis with the element Ag in the sump pool. These reactions are controlled by the mass transfer of I_2 and I^- within the pool and the degree of oxidation in the dissolved silver.

From the experimentally measured data, it appears that the direct formation of gaseous iodine from the pool and the effect of oxidation for Ag in the formation of AgI were negligible. The iodine and silver transpired to be insoluble in the sump, but Cs was a very soluble element. Te showed a low solubility in water. The massive formation of AgI in the sump pool can inhibit molecular iodine from forming by radiolysis, partitioning from the pool, moving into the atmosphere. Therefore, these results from the FPT-1 test show that the sump plays an important role as an iodine sinker and the AgI was a stable chemical compound under radiation.

In accordance with the results from the Phebus FPT-1 test, MELCOR considers silver as a sinker for iodine and AgI as a stable compound under radiation. But MELCOR limits the maximum mass of the silver that can combine with the iodine to a 10^{-6} fraction of the existing silver in the pool. The issues that remain are the development of the reaction equations to form a silver iodide and their reaction constants in the iodine pool chemistry model in MELCOR. These days most of the nuclear power plants are not adopting silver-indium-cadmium but boron carbide (B_4C) as a control rod absorber material. Therefore, it is also necessary to study the effect of boron carbide on the trapping of iodine within the pool [14].

3. CONCLUSIONS

The vast amount of data produced from the Phebus FP program provides a valuable database for validating the severe accident codes. Moreover, many important new issues concerning reactor safety were identified through this program. The new issues identified include the violent oxidation and volatility of ruthenium-oxide by the air ingress, B_4C control rod failure and its oxidation, the different fission product release patterns from the high burn-up fuel (40 > GWD/MTU) and new types of fuel such as MOX, and finally, the organic iodine generation area through the complex iodine chemistry in the containment. However, the data currently available are not sufficient for modeling the above-mentioned phenomena.

One of the important lessons learned from this study was the effect of a high fuel burn-up on the core damage and the fission product behavior. As a high burn-up of fuel is becoming more and more favored internationally, it is recommended that the current models in severe accident codes be reviewed to validate them under a high fuel burn-up condition.

Through this study, MELCOR was found to be useful for predicting the thermal hydraulic and fission product behaviors not only for a real power plant, but also for an arbitrarily designed experimental facility such as that use in the Phebus FPT-1 test. Especially, the user-supplied sensitivity cards allow the model uncertainty to be assessed and the separate effects of the corresponding parameters to be identified. In addition, the complex experimental boundary and initial conditions in the various parts of the test facility were easily prepared using the control functions in the MELCOR code.

Even though MELCOR has a full set of models and functions for analyzing accident progression under severe accident conditions, many models were still identified as insufficient or absent from this study. They are as follows:

- Need to apply multiple calculation points for the fuel cross section to develop a more refined model for a high fuel burn-up.
- Validate the Zr oxidation kinetic correlation by the air ingress into the core.
- Adopt the eutectic model and its validation as the default.
- Include a B_4C control rod failure mode and the release of its absorber material. (This has been included in MELCOR 1.8.6.)
- Remedy the absence of an iodine chemistry model in the RCS circuit to identify chemical forms, especially the gaseous iodine compounds.
- Control the over-estimation of fission product aerosol depositions on the cold section using the thermo-phoresis phenomenon.
- Remedy the absence of an organic iodide generation model from not only the water pool, but also the atmosphere.
- Include the new issues regarding the high burn-up fuel and implement the new material properties for advanced reactors such as HTGR.

ACKNOWLEDGEMENT

We would like to thank Dr M. Schwarz who is in charge of the Phebus FP experiment and all those in IRSN who have been involved in this experimental program. Also, we would like to thank MOST for supporting this research within the frame of MOST's long term R&D program.

REFERENCES

[1] J.C.Nimal,B. Nimal, B.Duchemin, "*Note de principe du Code PEPIN*", CEA Report, DEMT 86/452, (1986).

[2] K.I. Ahn, D.H.Kim, "*Development of a Database System for the Support of Severe Accident Risk Management*", The sixth international conference on probabilistic safety assessment and management, San Juan USA, (2002).

[3] A. Mailliat, "*STLOC Source Term Part Phebus 2000 Feasibility Study Summary*", IRSN, (2003).

[4] D. Jacquemain, S. Bourdon, Anne de Bremaecker, M. Barrachin, "*FPT-1 Final Report: vol 1~4*", IRSN/DRS/SEA/PEPF, (2000).

[5] G. Repetto, "*Results and Analysis of the FPT-0, FPT-1, FPT-2 and FPT-4 Experiments of the Phebus FP program investigating In-Vessel Phenomena during a LWR Accident*", Seminar at KAERI, (2003).

[6] B. Clement, N.Hanniet-Girault, G.Repetto, D.Jacquemain, A.V.Jones, M.P. Kissane, P.von der Hardt, "*LWR severe accident simulation: synthesis of the results and interpretation of the first Phebus FP experiment FPT0*", Nuclear Engineering and Design 226 5-82, (2003).
[7] R.O. Gauntt, "*Current MELCOR Development Activities*", MCAP-2003 Meeting , Bethesda MD, (2003).
[8] B. Clement, T. Haste, "*ISP-46 Status: May 2003*", CSARP Meeting, Bethesda, (2003).
[9] J.H Park, D.H Kim, "*The comparison of FP deposition on SG U-tubes between lumped and 1-D model with consideration of temperature and velocity gradient by thermophoresis phenomena*", 2003 KNS autumn conference, (2003).
[10] Parker C. Reist, "*Aerosol Science and Technology*," McGraw-Hill, 2nd edition, (1992).
[11] Edurrdo Honaiser, Samim Anghaie, "*FPTRAN: A Volatile Fission Product and Structural Materials Transport Code for SCDAP/RELAP5*", ICAPP 04, Pittsburgh, PA USA, (2004).
[12] A.L. Wright, S. Adroguer, et al., "*Primary System Fission Product Release and Transport*," NUREG/CR-6193 NEA/CSNI/R(94)2 ORNL/TM-12681, Oak Ridge, (1994).
[13] N. Girault, et al., "*Phebus-FP Containment Chemistry Interpretation Circle: FPT-1 Final Interpretation Report*", Note Technique DPAM/SEMIC Phebus FP/IP 03-545, (2004).
[14] M Schwarz, B. Clement, "Proposal for a cooperative Research Program on Severe Accidents: Source Term separate-effect tests program", Meeting material at Paris, (2005).